THE ASTROPHYSICAL JOURNAL, 566:1124–1131, 2002 February 20

CONSTRAINTS ON CIRCUMSTELLAR DISK PARAMETERS FROM MULTIWAVELENGTH OBSERVATIONS: T TAURI AND SU AURIGAE

R. L. AKESON,[1,2] D. R. CIARDI,[3] G. T. VAN BELLE,[2] AND M. J. CREECH-EAKMAN[2]
Received 2001 August 22; accepted 2001 October 22

ABSTRACT

We present circumstellar disk models for two pre–main-sequence objects, T Tau and SU Aur. The models are based on interferometric data from infrared and millimeter wavelengths and infrared photometry from the literature. The physical properties of the disk are examined by calculating parameter probabilities based on a passive, flat-disk model. The model adequately fits the data for SU Aur but not for T Tau. We find that there are significant differences in the physical parameters suggested by the individual data sets. The size of the inner disk radius as implied by the infrared interferometry data ($\sim$tenths of AU) is larger than expected for a flat-disk model. This discrepancy is discussed in consideration of more complex disk models that include the presence of a hot, inner region or wall in the disk.

Subject headings: circumstellar matter — stars: individual (T Tauri, SU Aurigae) — stars: pre–main-sequence

1. INTRODUCTION

The formation of a circumstellar disk is a crucial stage in the canonical model of low-mass star formation. These disks play a key role in the transfer of material onto the central star and are the reservoir of material from which planetary systems are formed. In the T Tauri stage, most sources are observed to have some disk characteristics. For example, Osterloh & Beckwith (1995) found that roughly 50% of the classical T Tauri stars they surveyed for millimeter-wave emission have disks, and Haisch, Lada, & Lada (2001) calculated a disk fraction of 70% for Taurus sources from mid-infrared excesses. As most or all of the circumstellar envelope has been dispersed by this stage in the star formation process (Mundy, Looney, & Welch 2000), these stars are particularly good candidates for studying disk properties.

Dust grains in the disk are the source of infrared emission in excess of photospheric emission and of the far-infrared and millimeter flux and are, therefore, a good tracer of the disk structure. Simple power-law models are often used to describe the physical properties such as the temperature and density distributions. These models generally rely upon fitting data from a limited wavelength range, which correspond to a limited temperature range and spatial scale in the disk or on spatially unresolved data such as infrared photometry. For example, millimeter-wave images are sensitive primarily to the outer, cooler section of the disk, while the near-infrared spectral energy distribution (SED) is dominated by the inner, hot regions. The advent of infrared interferometry has allowed spatially resolved observations of the inner disks. Akeson et al. (2000, hereafter Paper I) presented observations of T Tau and SU Aur that demonstrated that the infrared emission from these sources was resolved on a scale of a few milliarcseconds. In this paper we present circumstellar disk models for these stars derived from data at infrared and millimeter wavelengths.

[1] Interferometry Science Center, California Institute of Technology, MS 100-22, Pasadena, CA 91125.

[2] Jet Propulsion Laboratory, California Institute of Technology, MS 171-113, 4800 Oak Grove, Pasadena, CA 91109.

[3] University of Florida, 211 Bryant Space Sciences Building, Gainesville, FL 32611.

2. OBSERVATIONS AND RESULTS

2.1. *Sources*

The T Tauri system, one of the best-studied pre–main-sequence objects, comprises T Tau N, an optically visible T Tauri star and T Tau S, an optically obscured infrared companion 0.″7 to the south. Recent observations (Koresko 2000) have revealed that T Tau S is a binary with a separation of 50 mas. The millimeter wave flux is dominated by material surrounding T Tau N and is consistent with circumstellar disk models with an outer radius of 40 AU (Akeson, Koerner, & Jensen 1998). Our infrared observations are also concentrated on T Tau N, and it is the disk around this component that we discuss here. SU Aur has an SED similar to that of T Tau N, and Herbig & Bell (1988) classified SU Aur separately from other weak-line T Tauri stars owing to its high luminosity and broad absorption lines.

2.2. *Palomar Testbed Interferometer*

In addition to using the data given by Paper I, we have obtained further infrared interferometric data on T Tau N and SU Aur. All observations were made in the K band (2.2 μm) at the Palomar Testbed Interferometer (PTI) on both the north-south ($\sim$110 meter) and north-west ($\sim$85 meter) baselines. PTI is described in detail in Colavita et al. (1999). The data were obtained on four nights in 2000 October and November and calibrated using the standard method described in Boden et al. (1998). A synthetic wideband channel is formed from the five spectrometer channels. The instrumental response to a point source is measured with respect to calibration stars. The same calibrators were used for both T Tau N and SU Aur in the 2000 observations, and the main calibrator (HD 28024) has been used in all observations (Paper I and those presented here). Calibrator sizes were estimated using a blackbody fit to photometric data from the literature. Calibrators are chosen by their proximity to the sources and for small angular size in order to minimize systematic errors in deriving the system visibility. All calibrators used in this reduction have angular diameters less than 0.8 mas and were assigned uncertainties of 0.1 mas. All nights contained more than one calibrator, and the sizes were confirmed to be internally consistent. The

data are presented in normalized squared visibility (which we will refer to as visibility hereafter), where an unresolved source has $V^2 = 1$. The uncertainties given for the calibrated visibilities are a combination of the calibrator size uncertainty and the internal scatter in the data.

For T Tau, an additional calibration must be applied to compensate for the incoherent contribution from T Tau S. As the telescope tracking at PTI is done at optical wavelengths, where T Tau N is the only observed component (Stapelfeldt et al. 1998), T Tau N is the component that is tracked and for which fringes are detected. As detailed by Paper I, the measured visibility must be corrected for the T Tau S incoherent contribution. T. Beck (2000, private communication) measured T Tau S/T Tau N flux ratios of 0.37 ± 0.02 on 2000 October 9 and 0.41 ± 0.02 on 2000 November 10. Our data were taken on four nights, all of which fall within 7 days of these observations, and we therefore use the ratio closest in time to each of our nights. These corrections are simply scalings for each night, and the corrected visibility corresponds to T Tau N alone.

The calibrated visibilities, combined with those from Paper I, averaged by hour angle and plotted against the baseline position angle on the sky, are shown in Figures 1 and 2. The projected baseline length changes by less than 10% for the observations shown here. Both sources clearly have a visibility less than 1, which can arise from a resolved source or from multiple sources of emission within the field of view, such as a binary companion. At the distance to the Taurus cloud ($\sim$140 pc) a star with a stellar radius of a few $R_\odot$ (typical for T Tauris) would have an angular diameter of less than 0.1 mas, which is not resolvable at PTI. Below we examine the various scenarios that could produce the measured visibilities.

First, the possibility that the observed visibilities arise from a binary companion is discussed. Although there are no known companions that would produce the measured

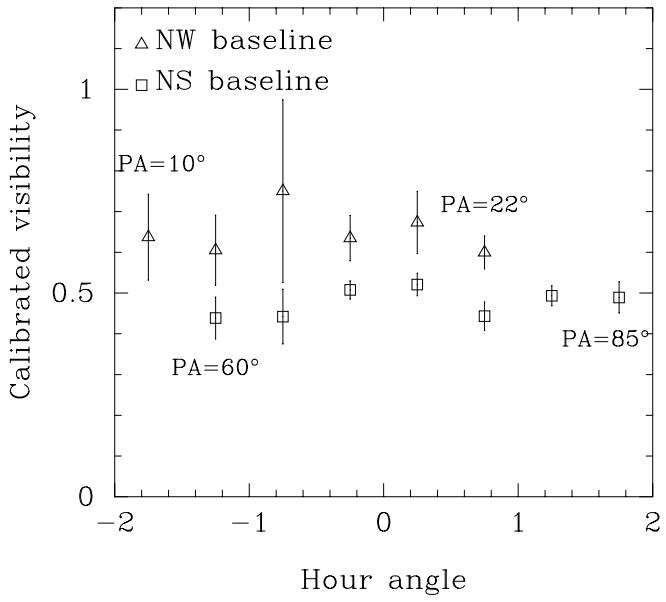

FIG. 1.—Calibrated squared visibilities for T Tau N from PTI separated by baseline and averaged by hour angle. The position angle of each baseline is marked. The baseline lengths range from 103 to 108 m (47–49 Mλ) for the north-south baseline and 83–86 m (38–39 Mλ) for the north-west baseline. The visibilities have been corrected for the incoherent contribution from T Tau S.

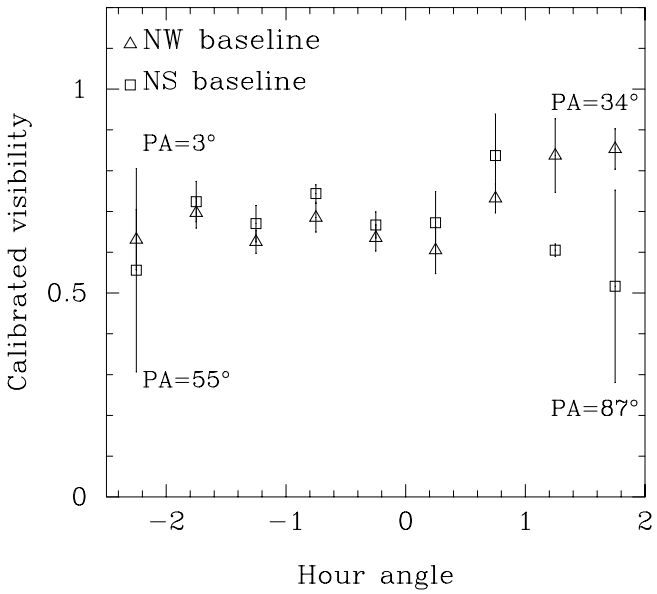

FIG. 2.—Calibrated squared visibilities for SU Aur from PTI separated by baseline and averaged by hour angle. The position angle of each baseline is marked. The baseline lengths range from 108 to 110 m (49–50 Mλ) for the north-south baseline and 78–86 m (35–39 Mλ) for the north-west baseline.

visibilities (see discussion of T Tau S above), there may be unknown companions on small spatial scales. A second source will produce a binary fringe pattern if the separation is within the coherence length, which for the data presented here corresponds to roughly 100 mas. The binary fringe pattern is a function of the projected baseline length and the binary separation vector. A close (separation <100 mas) orbiting companion would produce significant visibility evolution with changes in the projected baseline and with time. For example, a $\sim 1\ M_\odot$ companion at a separation of 10 mas would have a period of $\sim$1 yr. For both sources, there are no visibility changes in time within the uncertainties, which suggests the visibility reduction is not due to a close orbiting companion. A chance superposition on the sky is unlikely given the small angular scales involved and would also produce visibility changes with projected baseline.

The source visibility can also be reduced by an incoherent contribution from a companion outside the coherence length. We know that this is the case for T Tau, which is corrected as discussed above. For SU Aur, the Ghez, Neugebauer, & Matthews (1993) speckle survey rules out a companion that would contribute sufficient incoherent flux to produce the observed visibility. Given the above arguments, we conclude that it is unlikely that the observed visibilities are due to unknown binary companions. We attribute the resolved visibility as arising from a combination of an unresolved photosphere and a circumstellar component.

The first step in using the observed visibility to study the disk properties is to remove the photospheric contribution, which was done with the following procedure. A blackbody curve with a temperature appropriate for the stellar type (5250 K for T Tau N and 5860 K for SU Aur) was fitted to *UBV* photometry to obtain the stellar luminosity, which was then subtracted from the infrared photometry. At *K* band, this resulted in a photospheric contribution of 28% for T Tau N and 27% for SU Aur.

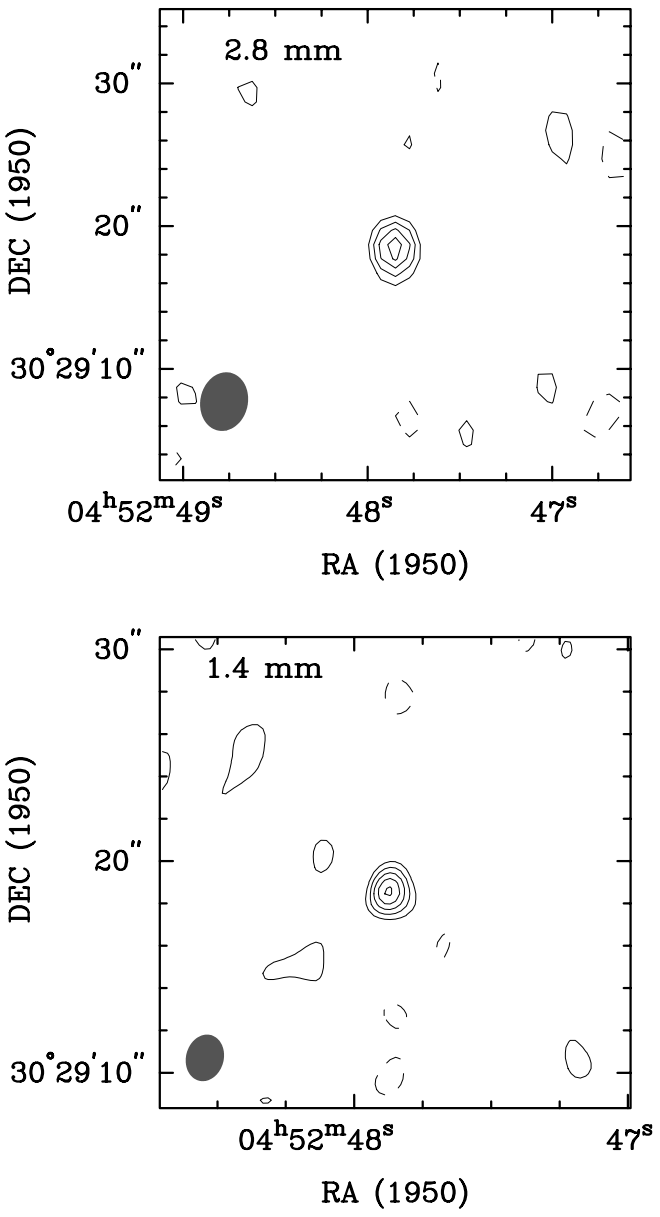

FIG. 3.—Millimeter wave continuum emission image of SU Aur. The contour levels are 1 σ (*top*, 1.7 mJy beam^{-1}; *bottom*, 2.6 mJy beam^{-1}) starting at 2 σ. The peak emission is 9.7 mJy beam^{-1} at 2.8 mm and 16 mJy beam^{-1} at 1.4 mm.

An estimate of the *K*-band emission region size comes from fitting the visibilities as a function of hour angle with a Gaussian brightness profile inclined on the sky. For T Tau N, the best fit has a FWHM of $1.54^{+0.05}_{-0.06}$ mas (0.22 AU) at an inclination angle of $29^{\circ}{}^{+10^{\circ}}_{-15^{\circ}}$ and position angle $132^{\circ}{}^{+13^{\circ}}_{-20^{\circ}}$. For SU Aur, the best fit has FWHM of $1.05^{+0.08}_{-0.07}$ mas (0.13 AU) at an inclination angle of $62^{\circ}{}^{+4^{\circ}}_{-8^{\circ}}$ and position angle $127^{\circ}{}^{+8^{\circ}}_{-9^{\circ}}$. The physical sizes are given for a distance of 140 pc.

TABLE 1

OVRO OBSERVATION RESULTS FOR SU AUR

Wavelength (mm)	Peak (mJy)	rms (mJy)	Beam Size (FWHM) (arcsec)	Beam P.A. (deg)
1.4	16	2.6	2.1 × 1.7	−25
2.8	9.7	1.7	4.0 × 3.2	−22

2.3. *Owens Valley Millimeter Array*

Millimeter-wave interferometry observations of SU Aur were taken with the Owens Valley Radio Observatory (OVRO) Millimeter Array on 2000 September 26 and October 17 in the low-resolution configuration. The wideband correlator was configured to obtain simultaneous continuum data at 1.4 and 2.8 mm with a 1 GHz channel in each sideband at each frequency. The two sidebands at each frequency were combined. The data were gain- and flux-calibrated with the MMA package. The absolute flux calibration was performed against previously measured flux values for 3C 273, 3C 84, and 3C 454.3. The continuum data were deconvolved and imaged using CLEAN in the DIFMAP package (Shepherd 1997) and are shown in Figure 3. The emission is unresolved at both wavelengths with beam sizes of 2.″1 × 1.″7 at 1.4 mm and 4.″0 × 3.″2 at 2.8 mm. The observation parameters and results are given in Table 1.

3. CIRCUMSTELLAR DISK MODELS

3.1. *General description*

We propose a model for these sources consisting of a star and a circumstellar disk, in which the infrared through millimeter emission arises entirely from the stellar photosphere and disk thermal emission. At millimeter wavelengths, the continuum emission from T Tauri stars is consistent with dust emission (see, e.g., Beckwith et al. 1990). In the near-infrared, the SED produced by an accretion disk is similar to that of a passive disk with only thermal emission for typical accretion rates of T Tauri stars ($\sim 10^{-8}\ M_{\odot}$ yr^{-1}; Kenyon & Hartmann 1987), so we will neglect accretion. To characterize the properties of the disk, infrared and millimeter interferometric data are used, along with infrared photometry from the literature. We have chosen not to include any far-infrared flux measurements, such as *IRAS*, as these observations are taken on much larger spatial scales and may include emission from other nearby sources.

For the disk, we have chosen a geometrically flat, symmetric disk model with flux, S_{ν}, in an annular ring at radius, r, given by

$$dS_{\nu}(r) = \frac{2\pi \cos(\theta)}{D^2} B_{\nu}(1 - e^{-\tau}) r dr\ , \qquad (1)$$

where θ is the inclination angle, D is the distance, and B_{ν} is the Planck function. The temperature and surface density are described as power-law functions of the radius ($T(r) = T_{10\ \mathrm{AU}}(r/10\ \mathrm{AU})^{-q}$ and $\Sigma(r) = \Sigma_{10\ \mathrm{AU}}(r/10\ \mathrm{AU})^{-p}$ with the reference points set at 10 AU. The dust opacity is given by a power-law function of the wavelength [$\kappa_{\nu} = \kappa_0(\nu/\nu_0)^{\beta}$]. The model is specified in terms of the optical depth,

$$\tau(r, \nu) = \frac{\Sigma\kappa_{\nu}}{\cos(\theta)} = \tau_{10\ \mathrm{AU}}\left(\frac{r}{10\ \mathrm{AU}}\right)^{-p}\left(\frac{\nu}{\nu_0}\right)^{\beta}. \qquad (2)$$

The dust opacity reference value (κ_0) is 0.1 g^{-1} cm^2 at $\lambda = 250\ \mu$m ($\nu_0 = 1200$ GHz; Hildebrand 1983).

A flat-disk model is used partially to keep the computational problem tractable and to examine if a flat disk can describe the data. Several groups have examined flared disks as both a natural feature of passive disks and as a way

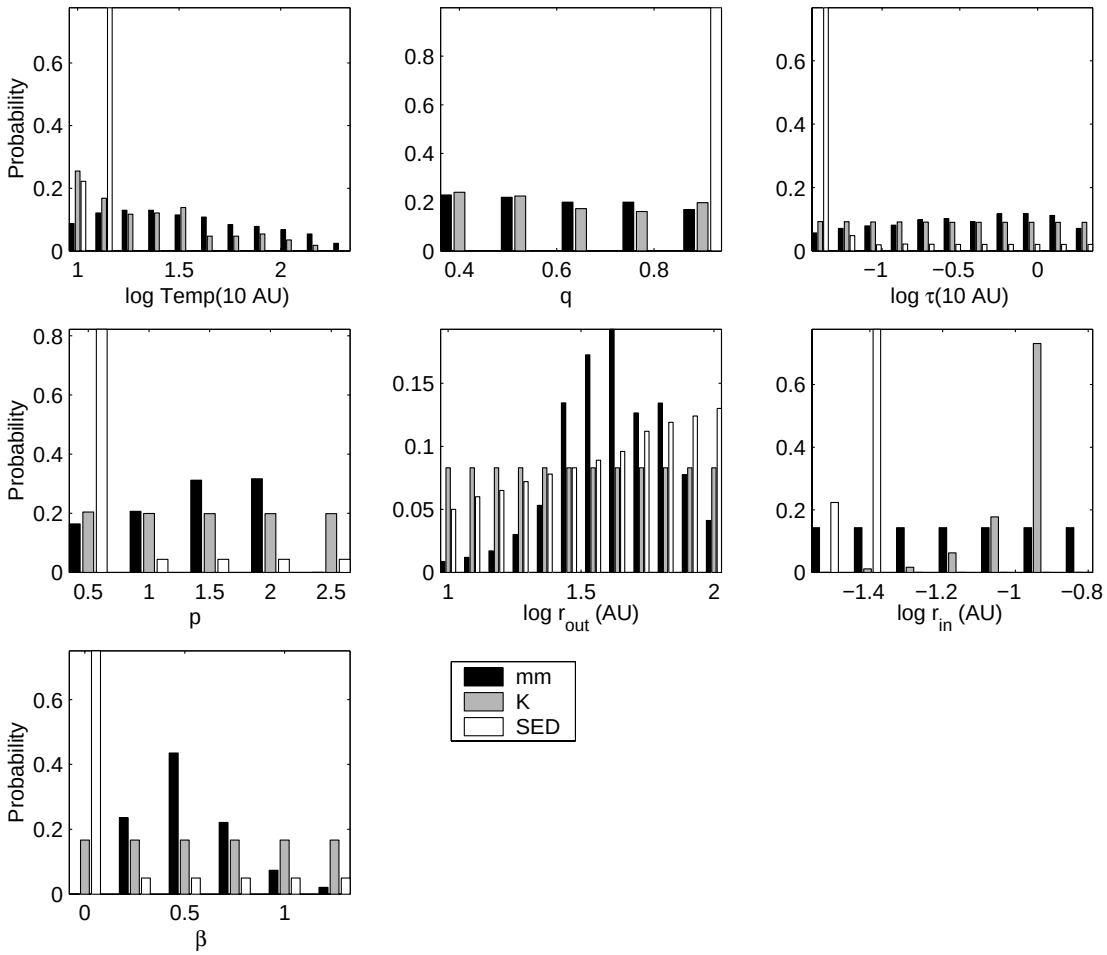

FIG. 4.—Parameter probabilities for models of the T Tau N data. Separate probabilities are shown for the millimeter data (*black*), *K*-band interferometry (*gray*), and infrared SED (*white*).

of explaining the flat infrared energy distributions of some T Tauri stars (see, e.g., Kenyon & Hartmann 1987; Chiang & Goldreich 1997). Flared disks arise from the influence of the stellar radiation on the disk material. In the Chiang & Goldreich (1997) model, the millimeter emission is dominated by the disk interior. The main observational difference in the millimeter regime between the Chiang & Goldreich (1997) models and a flat disk is that the flat disk predicts a shallower spectral slope. In the infrared, however, the shape of the SEDs predicted for flat and flared disks are dramatically different, and it may certainly be possible to fit the infrared SEDs of our sources more closely with a flared disk model. More complex disk models are further discussed in § 4.

The model has a total of nine parameters: $T_{10\,\mathrm{AU}}$, q, $\tau_{10\,\mathrm{AU}}$, p, the disk outer and inner radii, r_{out} and r_{in}, β, the disk inclination, and position angles. A range of values was used for each parameter with logarithmic spacings for the temperature, optical depth, and inner and outer radii. The final range of values for each parameter is given in Table 2. Wider ranges were considered initially to find the applicable regions of parameter space. For each set of parameter

TABLE 2

PARAMETER VALUE RANGES IN MODEL FITS

	T TAU N				SU AUR			
Parameter	Total Range	Millimeter	*K* band	SED	Total Range	Millimeter	*K* band	SED
$T_{10\,\mathrm{AU}}$ (K).....	10–200	15–83	11–50	13	20–150	23–73	25–80	25–71
q	0.4–0.9	...	...	0.90	0.5–1.0	0.53–0.74	0.54–0.77	0.63–0.92
$\tau_{10\,\mathrm{AU}}$	0.04–2.0	0.09–1.0	...	0.04	0.002–0.5	0.01–0.05	...	0.002–0.016
p	0.5–2.5	0.9–2.0	...	0.5–1.3	0.5–2.0	0.74–1.64	...	0.57–1.25
r_{out} (AU)	12–100	27–64	...	17–75	50–400	70–240	...	...
r_{in} (AU)	0.03–0.15	...	0.09–0.12	0.03–0.05	0.04–0.1	...	0.05–0.08	0.05–0.09
β	0–1.25	0.28–0.77	...	0	−1.0–0.25	−0.88–0.24	...	−0.42–0.16

NOTE.—The step sizes are shown in Figs. 4 and 6. The parameter value ranges in the millimeter, *K* band, and SED columns are for the values encompassing 68% of the probability around the median value. Parameters for which all values are equally likely are indicated by (...).

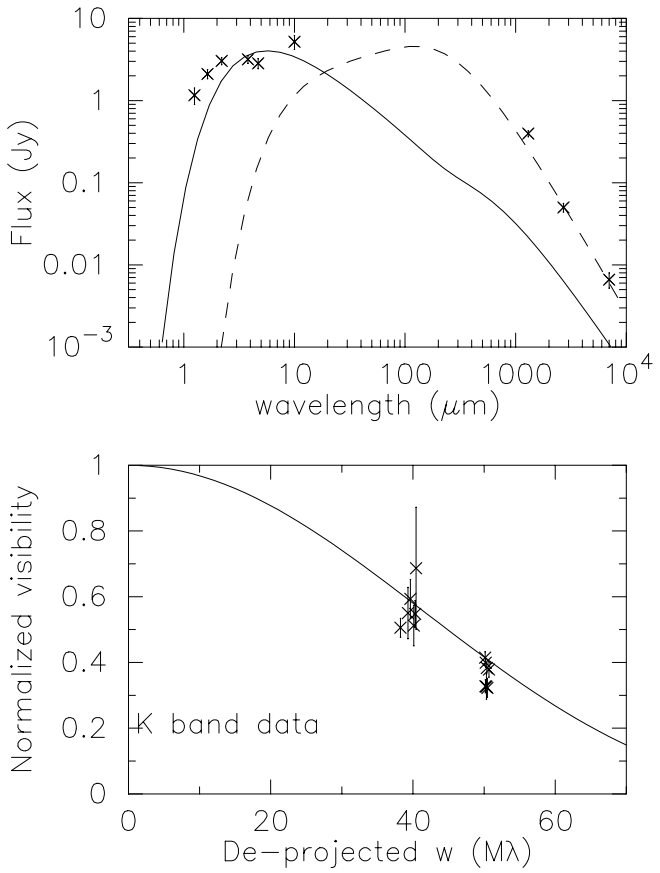

FIG. 5.—Representative disk model fits to the SED data and millimeter data for T Tau N. The stellar photosphere contribution has been removed. *Top*: The SED and millimeter flux data (*points*) and model fluxes (*lines*). Two models are shown: one that fits the SED (*solid line*), and one that fits the millimeter data (*dashed line*). The millimeter data were fitted as visibilities, although they are shown here only as total flux points. The model parameters (*solid/dashed lines*) are $T_{10\,\mathrm{AU}} = 18/30$ K, $q = 0.9/0.6$, $\tau_{10\,\mathrm{AU}} = 0.04/0.5$, $p = 0.5/1.5$, $r_{\mathrm{out}} = 55/45$ AU, $r_{\mathrm{in}} = 0.07/0.07$ AU, $\beta = 0/0.5$, inclination angle = 30°/30°, position angle = 20°/20°. *Bottom*: The deprojected K-band data and model. The parameters are the same as for the SED model except with $T_{10\,\mathrm{AU}} = 30$ K, $q = 0.77$, $r_{\mathrm{in}} = 0.12$ AU, and position angle = 130°. The error bars are 1 σ.

values, model visibilities and fluxes are derived and a standard χ^2 difference between the model and data points was calculated.

Rather than simply find the best model, we have characterized the disk parameters by calculating a probability distribution for each parameter. This method is used for two reasons: first, the probabilities show how well a given parameter is constrained, and second, this allows comparison of the probabilities among subsets of the data. The probability of a particular model, given the data, is proportional to $e^{-\chi^2}$. The probability is calculated separately for each data set, and the probability for the total data set is the product of these individual probabilities. For each parameter value, the relative probability is the sum of all probabilities for the range of values in all the other parameters. More detail on this Bayesian approach is given in Lay, Carlstrom, & Hills (1997).

The model parameters derived here are not necessarily unique but are used to examine which observations constrain which parameters. It should be noted that the parameter probabilities calculated apply only to this disk model and its assumptions and do not evaluate how well other models might describe the data. Our approach neglects any contribution to the data from an extended envelope. Akeson et al. (1998) found no evidence for an envelope component (emission on scales of hundreds of AU) in their millimeter data on T Tau N, although Hogerheijde et al. (1997) required a small (0.005–0.003 $M_\odot$) circumbinary envelope to fit their SED.

SU Aur is not as well studied in this respect. The unresolved millimeter images presented in § 2.3 have beam sizes of 300 and 560 AU at 1.4 and 2.8 mm, and we cannot rule out emission on those scales. However, given that SU Aur is optically visible and that its SED is similar to other sources with strong evidence for disk structures, we will assume here that the infrared and millimeter flux arise primarily from a circumstellar disk.

3.2. *Data Used in Fits*

For both sources, we used millimeter and K-band interferometry and infrared photometry in deriving the disk parameters. The infrared interferometry data used are described in § 2.2. For T Tau N, we used the millimeter interferometry data at 1.3, 2.7, and 7 mm, as described in Akeson et al. (1998). For SU Aur, we used the 1.4 and 2.8 mm data as shown in § 2.3. The infrared photometry (1.2–10 μm) is taken from Ghez et al. (1991) for T Tau N and from Kenyon & Hartmann (1995) for SU Aur. For the N-band (10 μm) flux for T Tau N, we used the values measured away from the silicon emission feature. The photospheric emission was removed from the infrared photometry with the same stellar parameters as used for the PTI data (§ 2.2). The photometry was corrected for extinction using $A_v = 1.4$ for T Tau N and 0.9 for SU Aur (Kenyon & Hartmann 1995).

In order to utilize a symmetric Hankel transform for calculation of the model visibilities, the u and v spatial frequencies of the visibilities are "deprojected" for each disk inclination and position angle value being considered. The resulting visibilities are binned by $w = (u^2 + v^2)^{1/2}$. Model visibilities were calculated at the appropriate wavelength and w-value. For comparison to the PTI data, the model visibilities are normalized to 1. The infrared photometry for the model is calculated as the zero spatial frequency visibility.

For the millimeter and SED data, a flux scaling is added to account for possible overall scaling errors. The flux error used at millimeter wavelengths is $1\sigma = 10\%$, and the scalings are weighted using a Gaussian distribution. In the infrared, the flux errors are more complex as there may also be a component owing to intrinsic source variability. As the infrared photometry used here is not contemporaneous with the PTI data, potential variability is taken into account as part of the flux error. Both sources discussed here were studied for variability by Skrutskie et al. (1996) who found that the SU Aur variations were consistent with a change in extinction, while T Tau is redder when it is bright. We used the measured color relations to scale all infrared fluxes for a given model with the total scaling set by the measured K magnitude variation (Skrutskie et al. 1996). All flux scalings were given equal weights and the probabilities summed for a given model.

3.3. *T Tau N Results*

For the T Tau N data, the same parameter values were used as in Akeson et al. (1998). The summed probabilities

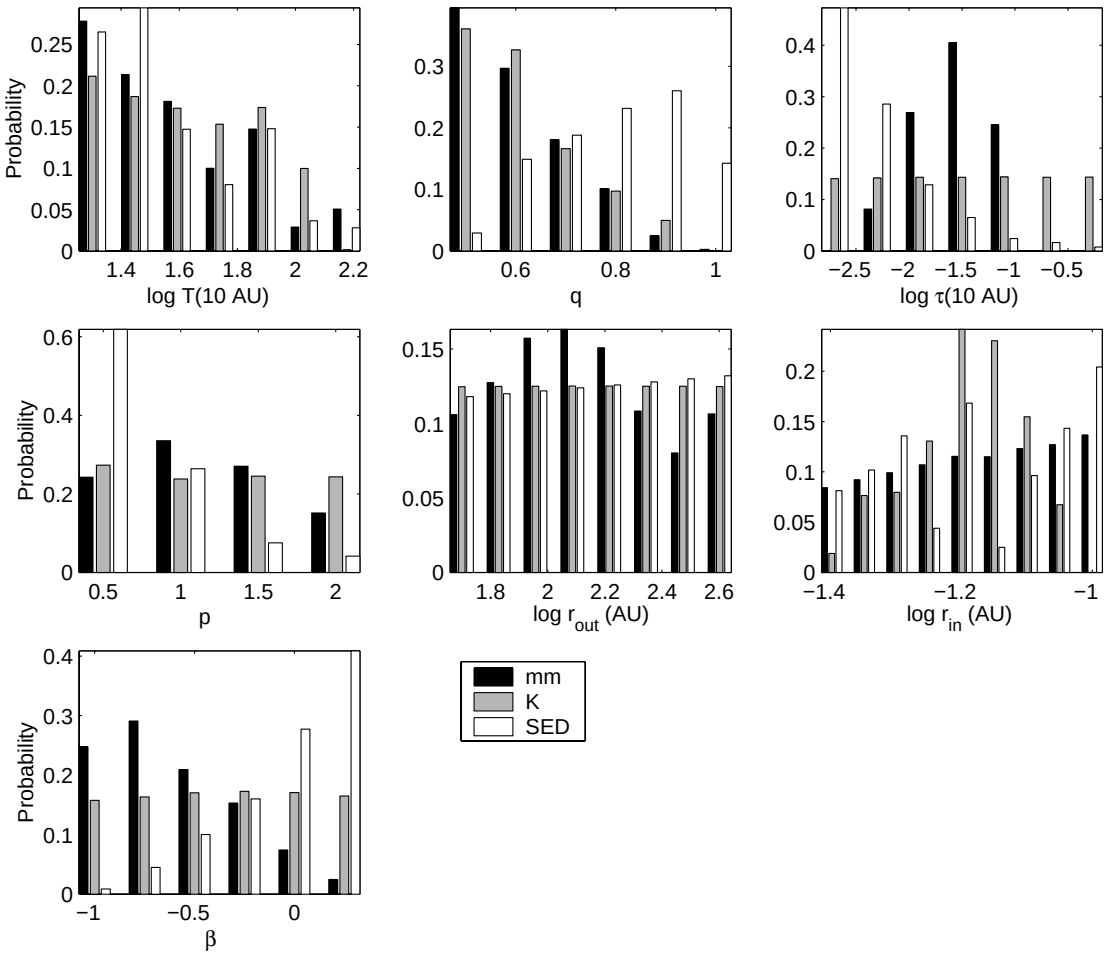

FIG. 6.—Parameter probabilities for models of the SU Aur data. Separate probabilities are shown for the millimeter data (*black*), *K*-band interferometry (*gray*), and infrared SED (*white*).

are shown in Figure 4. The position and inclination angles are not shown but are discussed below. To emphasize the differences between the data sets, the probabilities are plotted separately for the millimeter data, the infrared interferometry data, and the SED data. As expected, not all of the data affect all of the parameters equally; e.g., the SED data do not depend on the position angle, and the millimeter data are insensitive to the disk inner radius. The parameter values encompassing a probability range of 68% about the median are given in Table 2 for each of the three data sets.

Although this circumstellar disk model can fit each of the individual data sets reasonably well, the parameter probabilities are not the same (as seen in Fig. 4 and Table 2), suggesting that this model is not a good description of the entire data set. Example models are shown in Figure 5. In the top panel, the models are plotted against the infrared SED and the millimeter fluxes. In the bottom panel, the model is plotted against the deprojected PTI visibilities. Each model fits either the SED or the millimeter data well but is a poor fit for the other data set. The SED data well constrain the temperature and density parameters. This may be partially due to an incorrect treatment of the variability, as most of the photometry from the literature used by Skrutskie et al. (1996) do not resolve the T Tau N/S binary. The most probable parameter values from the SED data and the millimeter interferometry do not agree for the temperature, optical depth, and β. The SED data are best fitted with $\beta = 0$, while for the millimeter data $\beta > 0.25$.

The position angle is constrained only by the interferometry data but is not well determined. The Gaussian fit to the PTI data has a position angle $132^\circ{}^{+13^\circ}_{-20^\circ}$ (§ 2.2), while a fit to the 2.7 mm data gives $19^\circ \pm 5^\circ$ (Akeson et al. 1998). Given the errors in fitting the PTI data, which show little or no variation with hour angle, it is difficult to draw any conclusions from this disagreement. The inclination angles are $29^\circ{}^{+10^\circ}_{-15^\circ}$ from the PTI data and $41^\circ \pm 3^\circ$ for the 2.7 mm data.

3.4. *SU Aur Results*

The summed probabilities for SU Aur are shown in Figure 6. The position angle and inclination angle (not shown) are best constrained by the PTI data with values consistent with the Gaussian fit given in § 2.2. The parameter value ranges encompassing a probability range 68% about the median are given in Table 2. In general, there are a wide range of parameters that roughly fit the data set as a whole. Two examples are given in Figure 7. Both these models fit the SED and millimeter data at about the same level. One model is also shown against the deprojected (see § 3.2) PTI data. The disk parameters are degenerate in some limiting cases, and these results suggest that the data set on

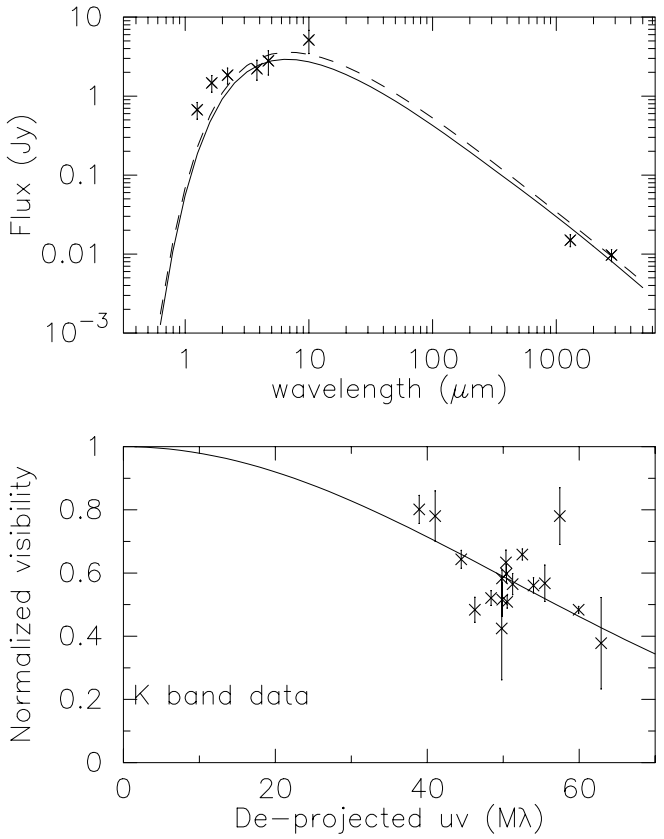

FIG. 7.—Representative model fits to the SED data and infrared interferometry for SU Aur. *Top*: The SED after subtraction of the stellar photosphere and two example models with parameters (*solid/dashed lines*) $T_{10\,\mathrm{AU}} = 55/150$ K, $q = 0.7/0.5$, $\tau_{10\,\mathrm{AU}} = 0.013/0.005$, $p = 1.5/2$, $r_{\mathrm{out}} = 400/50$ AU, $r_{\mathrm{in}} = 0.063/0.056$ AU, $\beta = -0.75/-1$, inclination angle = 53°/48°, and position angle = 130°/130°. The error bars are 1 σ. *Bottom*: The deprojected infrared interferometry data and model for the first model as above.

SU Aur is not sufficient to constrain the model parameters. However, some interesting trends are observed.

The temperature radial exponent from the millimeter and infrared interferometry data are generally lower ($q < 0.7$) than for the SED data ($q > 0.7$), while the SED data favor optically thin disks with shallow density radial profiles. The outer radius is not well constrained. This is not surprising as the millimeter images are not resolved.

The millimeter data are best fitted by $\beta < -0.25$, while the SED data are the opposite. For optically thin emission in the Rayleigh-Jeans regime, β can be calculated from the spectral index, $F_\nu \propto \nu^{2+\beta}$. For SU Aur, this value of β is -1.2 ± 0.35, which is lower than the typically observed values of $\beta = 0$–1 (Beckwith, Henning, & Nakagawa 2000). Including additional wavelengths would improve the estimate of β; however, there is a large discrepancy in the literature between different single-dish observations of the millimeter flux from SU Aur. The measured values of 72 ± 18 mJy beam^{-1} at 1.1 mm in a 15″ beam (Weintraub, Sandell, & Duncan 1989) and 21 ± 10 mJy beam^{-1} at 1.3 mm in an 11″ beam (Beckwith et al. 1990) would suggest an unreasonably high β ($\simeq 5$) if due to the wavelength difference alone. At these scales (1500 vs. 2100 AU), resolution of dust emission from an extended envelope is unlikely as the main cause for this discrepancy.

3.5. *Disk Masses*

For each set of model parameters, a disk mass can be derived. By binning the probabilities of these models by mass, we have calculated the mass probabilities. For T Tau N, the total disk mass from the millimeter data is $\log (M_D/M_\odot) = -2.4^{+0.7}_{-0.6}$, while the SED data have a median disk mass of $\log (M_D/M_\odot) = -4$. This difference is due to the dissimilar probabilities in the optical depth and β.

For SU Aur, the median disk mass using the probabilities from the total data set is $\log (M_D/M_\odot) = -5.1^{+1.4}_{-0.8}$, with similar median masses from the SED data and the millimeter data alone. This disk mass is considerably lower than for T Tau N. The Osterloh & Beckwith (1995) survey included two stars (other than SU Aur itself) classified as SU Aur types. Neither of these two stars was detected with an upper limit of 15 mJy at 1.3 mm. In general, Osterloh & Beckwith (1995) found that weak-line T Tauri stars have lower disk masses. This suggests that as a class of sources, SU Aur stars are similar to weak-line T Tauri in having less circumstellar material than classical T Tauri stars.

4. DISCUSSION

We have used a simple passive flat-disk model to study the emission from a wide range of spatial scales in the circumstellar disks of two T Tauri sources. We find that for one source, T Tau N, it is not possible to fit the entire range of data with this simple model. Subsets of the data for T Tau N can be fitted well with a flat circumstellar disk model; the millimeter emission was modeled by Akeson et al. (1998) while the infrared SED was modeled by Ghez et al. (1991). For SU Aur, it is possible to roughly fit all the data presented; however, the most likely parameter values vary across the data sets. A significant difference between the two objects is that SU Aur appears to have an optically thin disk as compared to T Tau N. In an optically thin disk some of the model parameters become degenerate (p and q, for example), allowing one set of parameter values to fit all the data.

Although a more complicated disk model is beyond the scope of this work, improvements in fitting all the data are clearly needed. One of the largest discrepancies apparent in our data is the inner disk radius. The infrared interferometry data directly measure the spatial scale of the K-band emission, and our data show size scales of tenths of AU for these sources (§ 2.2). The SED data also depend on the inner disk radius, but the values suggested by our fits either do not well constrain the inner radius (SU Aur) or prefer a value that is significantly smaller than the value suggested by the infrared interferometry (T Tau N).

Recent observations and theory work on the issue of inner disk structure have been done on Herbig Ae/Be (HAeBe) stars, the higher mass analogs of T Tauri stars. Millan-Gabet, Schloerb, & Traub (2001) observed 15 HAeBe stars with the Infrared Optical Telescope Array in the H and K bands and found that the characteristic sizes given by the visibilities were larger than expected. Their measured visibilities were generally more consistent with spherical envelopes or thin shells than with disk models. Tuthill, Monnier, & Danchi (2001) used aperture masking to image LkHα 101 also at H and K and found an inner edge for the infrared emission at 21 mas (3.4 AU if the distance is 160 pc), and they infer that this position is set by

dust sublimation. Theoretical work by Natta et al. (2001) to explain the discrepancy between near-infrared observations and models in HAeBe stars suggest that a thick inner wall is created at the dust sublimation radius.

In our models, the inner radius was a free parameter, constrained such that the temperature at that point was less than the dust sublimation temperature (which was conservatively set at 2000 K). Another approach would have been to set the inner radius at the point where dust condenses for the appropriate stellar temperature. This assumes that there is no optically thick material within this radius. Using a more typical dust condensation temperature of 1500 K, these radii are 0.11 AU for T Tau N and 0.14 AU for SU Aur, both within a factor of 2 of the simple Gaussian size scale fitted to the infrared interferometry (§ 2.2).

More physically developed disk models may address this discrepancy. Dullemond, Dominik, & Natta (2001) have extended the irradiated passive disk model of Chiang & Goldreich (1997) to include a vertically extended inner wall at the dust sublimation point. They find that for stellar parameters appropriate for a T Tauri star, the infrared SED is similar to that produced by a flat-disk model with little or no inner hole. Although the SED data for T Tau N and SU Aur can be well fitted by the simple flat-disk model, there is disagreement with the infrared interferometry measurements. The Dullemond et al. (2001) model can qualitatively account for both the SED and the interferometricly measured infrared size scales. If these models are correct, many T Tauri circumstellar disks may have substantially larger inner disk radii than as previously determined from SED fitting, as is suggested by the recent infrared interferometry observations. If T Tauri stars do have substantial inner disk holes, this has implications for such processes as disk-driven outflows and planet formation in the inner disk.

This work was performed at the Infrared Processing and Analysis Center and the Jet Propulsion Laboratory, California Institute of Technology. We are grateful to T. Beck for providing the T Tau flux ratios and for useful discussions on variability. Data were obtained at the Palomar Observatory using the NASA Palomar Testbed Interferometer, which is supported by NASA contracts to the Jet Propulsion Laboratory. Science operations with PTI are possible through the efforts of the PTI Collaboration (http://huey.jpl.nasa.gov/palomar/ptimembers.html), Jean Mueller and Kevin Rykoski. Observations at OVRO are supported by NSF grant AST 96-13717 to the California Institute of Technology.

REFERENCES

Akeson, R. L., Ciardi, D. R., van Belle, G. T., Creech-Eakman, M. J., & Lada, E. A. 2000, ApJ, 543, 313
Akeson, R. L., Koerner, D. W., & Jensen, E. L. N. 1998, ApJ, 505, 358
Beckwith, S. V. W., Henning, T., & Nakagawa, Y. 2000, in Protostars and Planets IV, ed. V. Mannings, A. P. Boss, & S. S. Russell (Tucson: Univ. Arizona), 533
Beckwith, S. V. W., Sargent, A. I., Chini, R. S., & Gusten, R. 1990, AJ, 99, 924
Boden, A. F., Colavita, M. M., van Belle, G. T., & Shao, M. 1998, Proc. SPIE, 3350, 872
Chiang, E. I., & Goldreich, P. 1997, ApJ, 490, 368
Colavita, M. M., et al. 1999, ApJ, 510, 505
Dullemond, C. P., Dominik, C., & Natta, A. 2001, ApJ, 560, 957
Ghez, A. M., Neugebauer, G., Gorham, P. W., Haniff, C. A., Kulkarni, S. R., Matthews, K., Koresko, C., & Beckwith, S. 1991, AJ, 102, 2066
Ghez, A. M., Neugebauer, G., & Matthews, K. 1993, AJ, 106, 2005
Haisch, K. E., Lada, E. A., & Lada, C. J. 2001, ApJ, 553, L153
Herbig, G. H., & Bell, K. R. 1988, Lick Obs. Bull. 1111, 1
Hildebrand, R. H. 1983, QJRAS, 24, 267
Hogerheijde, M. R., van Langevelde, H. J., Mundy, L. G., Blake, G. A., & van Dishoeck, E. F. 1997, ApJ, 490, L99
Kenyon, S. J., & Hartmann, L. 1987, ApJ, 323, 714
———. 1995, ApJS, 101, 117
Koresko, C. D. 2000, ApJ, 531, L147
Lay, O. P., Carlstrom, J. E., & Hills, R. E. 1997, ApJ, 489, 917
Millan-Gabet, R., Schloerb, F. P., & Traub, W. A. 2001, ApJ, 546, 358
Mundy, L. G., Looney, L. W., & Welch, W. J. 2000, in Protostars and Planets IV, ed. V. Mannings, A. P. Boss, & S. S. Russell (Tucson: Univ. Arizona), 355
Natta, A., Prusti, T., Neri, R., Wooden, D., Grinin, V. P., & Mannings, V. 2001, A&A, 371, 186
Osterloh, M., & Beckwith, S. V. W. 1995, ApJ, 439, 288
Shepherd, M. C. 1997, in ASP Conf. Ser. 125, Astronomical Data Analysis Software and Systems IV, ed. G. Hunt & H. F. Payne (San Francisco: ASP), 77
Skrutskie, M. F., Meyer, M. R., Whalen, D., & Hamilton, C. 1996, AJ, 112, 2168
Stapelfeldt, K. R., et al. 1998, ApJ, 508, 736
Tuthill, P. G., Monnier, J. D., & Danchi, W. C. 2001, Nature, 409, 1012
Weintraub, D. A., Sandell, G., & Duncan, W. D. 1989, ApJ, 340, L69